LANGMUIR

pubs.acs.org/Langmuir Article

Aerosol Synthesis of High Entropy Alloy Nanoparticles

Yong Yang, Boao Song, Xiang Ke, Feiyu Xu, Krassimir N. Bozhilov, Liangbing Hu, Reza Shahbazian-Yassar,* and Michael R. Zachariah*

Cite This: *Langmuir* 2020, 36, 1985−1992 Read Online

ACCESS | Metrics & More | Article Recommendations | Supporting Information

ABSTRACT: Homogeneously mixing multiple metal elements within a single particle may offer new material property functionalities. High entropy alloys (HEAs), nominally defined as structures containing five or more well-mixed metal elements, are being explored at the nanoscale, but the scale-up to enable their industrial application is an extremely challenging problem. Here, we report an aerosol droplet-mediated technique toward scalable synthesis of HEA nanoparticles with atomic-level mixing of immiscible metal elements. An aqueous solution of metal salts is nebulized to generate ∼1 μm aerosol droplets, which when subjected to fast heating/quenching result in decomposition of the precursors and freezing-in of the zero-valent metal atoms. Atomic-level resolution scanning transmission electron microscopy coupled with energy-dispersive X-ray spectroscopy analysis reveals that all metal elements in the nanoparticles are homogeneously mixed at the atomic level. We believe that this approach offers a facile and flexible aerosol droplet-mediated synthesis technique that will ultimately enable bulk processing starting from a particulate HEA.

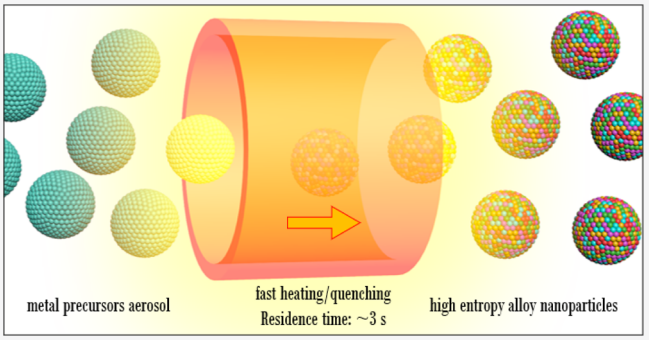

INTRODUCTION

Combining multiple metals into one single particle at the nanoscale enables the formation of multicomponent metal nanoparticles with unique physical and chemical properties.[1,2] The electronic interactions between different metal components make them potentially promising materials for a broad range of applications in the fields of catalysis, plasmonics, nanomedicine, and electronics.[3] Among all the multicomponent metallic nanostructures investigated, the attention on high entropy alloy (HEA) nanoparticles has been growing dramatically. HEAs represent such nanostructures, defined as five or more well-mixed metal elements in near equimolar ratios.[4] The maximized interactions between different metal atoms lead to the formation of the unique architectures with a high configurational entropy of mixing, resulting in advanced properties, including high mechanical strengths at high temperature, high corrosion resistance, and high oxidation resistance, among others.[5]

To date, primary techniques used to produce multicomponent metal nanoparticles, either in an alloyed or phase-separated state, are wet chemistry-based approaches, including bulk solution synthesis,[6] microfluidic method,[7] and micro-emulsion.[8] However, forming metallic nanostructures containing more than three metal elements using traditional wet chemistry approaches becomes challenging because of the increasing difficulty arising from balancing diverse reduction kinetics of different metal precursors. This often results in site-selective nucleation of each metal and the formation of nanoparticles with components and structures varying from particle to particle. In order to address this issue, a site-specific lithography-based synthesis technique has been recently reported to fabricate multicomponent metal nanoparticles containing five metal elements by confining the corresponding metal precursors in a small reaction volume on a desired site followed by hydrogen reduction procedures at elevated temperatures.[9] Although this technique has greatly expanded the composition and structure diversities of multicomponent metal nanoparticles, phase-separated nanostructures were always generated when incompatible metal elements (such as Cu and Co) were used. The reason is that the slow heating and slow quenching applied in hydrogen reduction procedures in this technique caused multicomponent nanoparticles to reach their thermodynamically favorable phase-separation state. Alternatively, melting processing has been developed to create bulk-size multicomponent alloys with uniformly mixed metal atoms, HEA, via melting and quenching physically mixed multiple metals.[10] However, a recent study on atomic distributions of the $Al_{1.3}$CoCrCuFeNi alloy generated via the melting technique reveals that Cu-rich precipitates were formed in the final product.[11] Furthermore, although melt

Received: October 31, 2019
Revised: January 30, 2020
Published: February 11, 2020

https://dx.doi.org/10.1021/acs.langmuir.9b03392
Langmuir 2020, 36, 1985−1992

processing has been successful in the synthesis of bulk HEAs as structural materials, generating HEAs at the nanoscale is extremely difficult with this technique.

We recently developed a carbothermal shock (CTS) technique to incorporate multiple immiscible metal elements into a single nanoparticle.[2] This technique involves an ultrafast electric heating step to thermally decompose carbon matrix-supported metal salt mixtures into liquid metal particles and a subsequent ultrafast quenching step to produce solid-state HEA nanoparticles containing well-mixed immiscible metal elements. With this technique, we were able to alloy up to eight metal elements into single-phase solid-solution nanoparticles uniformly dispersed on carbon supports. Although we have demonstrated the advantage of the technique over size and composition control on HEA nanoparticle synthesis, this joule heating-assisted thermal shock technique is limited to electrically conductive matrices and is not suitable for large-scale production of HEA nanoparticles.

Building on that work, we provide an aerosol droplet-mediated approach toward scalable synthesis of HEA nanoparticles with atomic-level mixing of immiscible metal elements. Although aerosol synthesis techniques have been extensively studied for manufacturing metals,[12] alloys,[13] metal oxides,[14] and composites,[15−18] here, we demonstrate the ability to make nominally unmixable materials in a manner amenable for bulk manufacturing quantities of HEA powders. Rather than predepositing metal salt mixture precursors onto a carbon support, we nebulize the precursors into aerosol droplets with a diameter less than 1 μm and employ a fast heating and fast quenching treatment. As such, each droplet contains precursors and operates as a nanoreactor, with very low thermal mass to enable rapid heating/cooling and small length scales to ensure no thermal and mass transfer gradients within the particle enabling one to produce a single HEA nanoparticle. We demonstrate the aerosol-mediated formation of five-element HEA nanoparticles containing Ni, Co, Cu, Fe, Pt, and Pd, chosen as example elements because of their applications in a broad range of fields including catalysis, magnetics, and electronics. Atomic-level resolution scanning transmission electron microscopy (STEM) coupled with energy-dispersive X-ray spectroscopy (EDS) analysis reveals that all metal elements (containing incompatible metals such as Co and Cu) in the nanoparticles are mixed together on an atomic level. The advantages of using an aerosol droplet-mediated technique are as follows: (1) all metal salts are preconfined into small droplets enabling incorporating different metals in the same particles during the heating and quenching process; (2) the small mass and volume nature of the aerosol droplets enables fast heating and fast cooling, which is crucially important to achieve kinetic control over the thermodynamic mixing regimes and creation of HEA nanoparticles; (3) metal salt ratios in the aerosol droplets reflect metal ratios in the precursor solution so that the component and composition of final products can be tuned by simply adjusting the type and ratio of metal salts in the precursor solution; and (4) because this technique is a continuous process, scaling-up will be greatly simplified.

RESULTS AND DISCUSSION

Methodology. Figure 1a exhibits a schematic of aerosol droplet-mediated approach toward scalable synthesis of HEA nanoparticles. Here, synthesis of NiCoCuFePt HEA nanoparticles is chosen to investigate synthesis−structure relationship. A detailed description including the reactor design and the operation parameters can be found in Experimental Section and in Figure S1. In a typical experiment, the precursor solution containing five types of metal salts with equal molar ratios mixed in de-ionized water was nebulized to create aerosol droplets using a Collison-type atomizer. The gas used to nebulize the solution was a 10% H_2/90% Ar reducing gas mixture to facilitate the formation of zero-valent HEAs. The nebulized aerosol droplets, carried by the gas mixture, were passed through a silica dryer for water solvent removal, and the resulting dried aerosol particles composed of five mixed metal salt species were carried through a high-temperature reaction zone (~1100 °C) in which a rapid temperature increase (thermal shock) triggers rapid thermal decomposition and hydrogen reduction of the metal salts to metal, leading to the formation of HEA nanoparticles upon fast quenching. Particles exiting the reactor were collected on a membrane filter collector. The calculated residence time of the aerosol particles in the heating zone based on the geometry of the reactor and the flow rate is about 3 s.

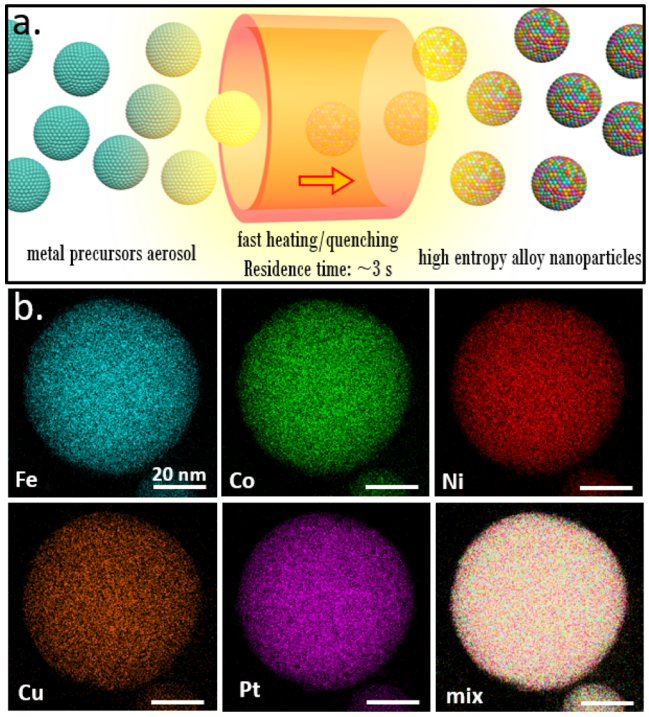

Figure 1. Aerosol droplet-mediated technique for scalable synthesis of HEA nanoparticles: (a) schematic of the evolution of aerosol droplets during the high-temperature treatment (note that the actual particle size is much smaller than the tube size shown in the cartoon) and (b) EDS mappings for a single HEA nanoparticle.

Figure 1b shows the elemental distributions within a single NiCoCuFePt HEA nanoparticle with a ~60 nm diameter. We observe that Ni, Co, Cu, Fe, and Pt elements are uniformly distributed in the nanoparticle and all five elements shown in the mixed EDS map are overlapped with each other, suggesting that HEA nanoparticles were successfully synthesized using the aerosol droplet-mediated approach. X-ray diffraction (XRD) pattern (Figure S2) on the bulk samples suggests that the synthesized particles have a single-phase structure without phase separation. This observation is further corroborated by the EDS data (Figure S3) which indicates that the main phase of the particle is metallic containing all five metals (Ni, Co, Cu,

https://dx.doi.org/10.1021/acs.langmuir.9b03392
Langmuir 2020, 36, 1985−1992

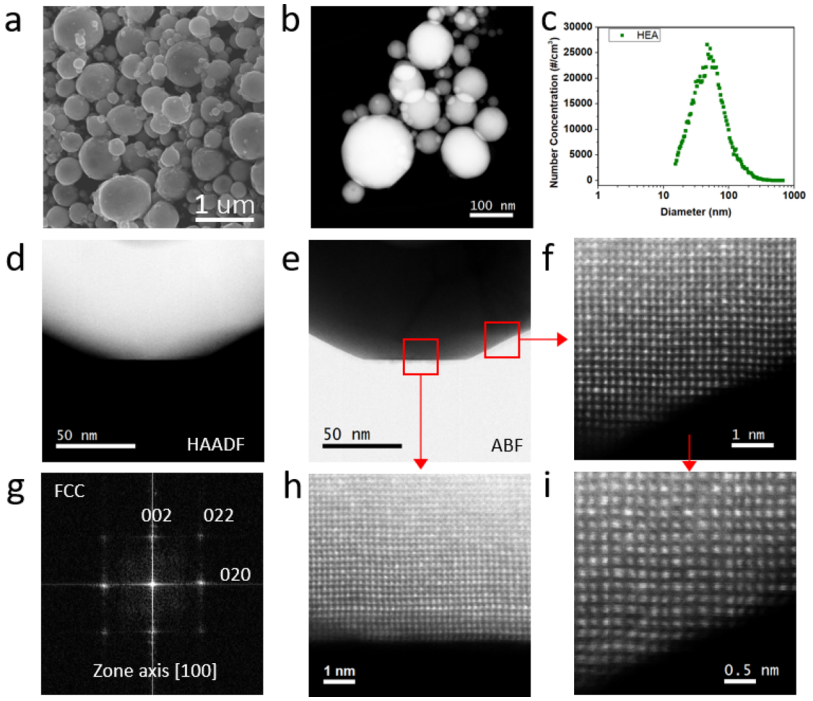

Figure 2. Morphology and microstructure of HEA nanoparticles: (a) SEM image of HEA nanoparticles; (b) low-magnification HAADF-STEM image of HEA nanoparticles; (c) size distribution of HEA nanoparticles measured using a DMA−CPC on-line size analysis system; (d,e) HAADF and ABF STEM for a single HEA nanoparticle; (f,h,i) atomic STEM image of the HEA nanoparticle; (g) FFT analysis of the HEA nanoparticle.

Fe, and Pt) with negligible oxygen content. The quantitative EDS analysis reveals that the composition of the HEA nanoparticle has deviated from the ideal composition with all five metals having a 20% atomic percentage. The atomic ratios in the synthesized nanoparticles are 19.16% for Ni, 19.19% for Co, 11.45% for Cu, 24.59% for Fe, and 25.60% for Pt. In particular, the percentage of Cu element is relatively low compared with the other metal elements in the nanoparticle. A similar result has also been observed on the HEA nanoparticles synthesized with the previously mentioned CTS approach.[2] The possible reason is the differences in vapor pressures between the various metals, with Cu having the highest vapor pressure (Figure S4). However, in our previous study, we employed a precursor compensation approach to balance the atomic ratio of volatile metals (i.e., add more of one component), which is a commonly used strategy when volatile metals are involved in the synthesis.[2]

The extremely small mass and volume of aerosol particles enable fast heating and quenching, which is crucially important to achieve kinetic control over the thermodynamic mixing regimes and creation of HEAs. The size of the dried aerosol particles containing multiple metal salts after water solvent removal was measured on-the-fly with a differential mobility analyzer (DMA) coupled with a condensation particle counter (CPC). The operation principles can be found in our previous publication.[19] The result shown in Figure S5 indicates that the aerosol distribution has an average size of 92.0 nm with a 1.77 geometric standard deviation. A simple heat transfer calculation indicates that a cold particle (25 °C) with a similar diameter can reach the ambient in a few nanoseconds once introduced into a high-temperature environment (1100 °C) and vice versa.[20] Therefore, the aerosol particles were always at the local gas temperature, and the heating and cooling rates of the aerosol particles became the heating and cooling rates of the aerosol gas flow in the tubular reactor. In order to estimate the temperature profiles of the gas flow in the tubular reactor, a finite-element simulation of the aerosol synthesis process was implemented using COMSOL Multiphysics software, and the result (Figure S6) suggests that the simulated temperature profile is consistent with the temperature measured using a thermocouple (Figures S7 and S8), and the heating and cooling rates of the flow were about 10^3 and 10^5 K/s, respectively, demonstrating the excellent fast heating and fast cooling nature of the aerosol process compared to the bulk batch reactors. In particular, the extremely high cooling rate is comparable to the cooling rate demonstrated in our CTS work. Achieving a high cooling rate is required to produce HEAs because slow cooling rates used in the previously reported techniques often cause multicomponent nanoparticles to reach their thermodynamically favorable phase-separation state (Figure S9). In our case, high cooling rates were achieved by thermophoresis on a cold surface.

Microstructure and Composition Analysis. Figure 2a,b shows the morphology of the HEA nanoparticles examined using scanning electron microscopy (SEM) and high-angle annular dark-field STEM (HAADF-STEM), respectively. The SEM image and the corresponding low-magnification HAADF-STEM image show that these particles have a spherical morphology. In order to check if these particles are a single sphere or agglomerates, we directly electrophoretically deposited particles exiting the reactor onto a TEM grid. The STEM images shown in Figure S10 show that particles are indeed single spheres. The lack of any discernible necking at these high temperatures (~1100 °C) and the fact that the calculated characteristic coagulation time is several orders of magnitude longer than the residence time or sintering time (see Figure S11) are consistent with this conclusion.

The size and concentration of the HEA nanoparticles were measured directly via an on-line DMA−CPC system. The concentration of the aerosol particles decreased from 2.5×10^6

https://dx.doi.org/10.1021/acs.langmuir.9b03392
Langmuir 2020, 36, 1985−1992

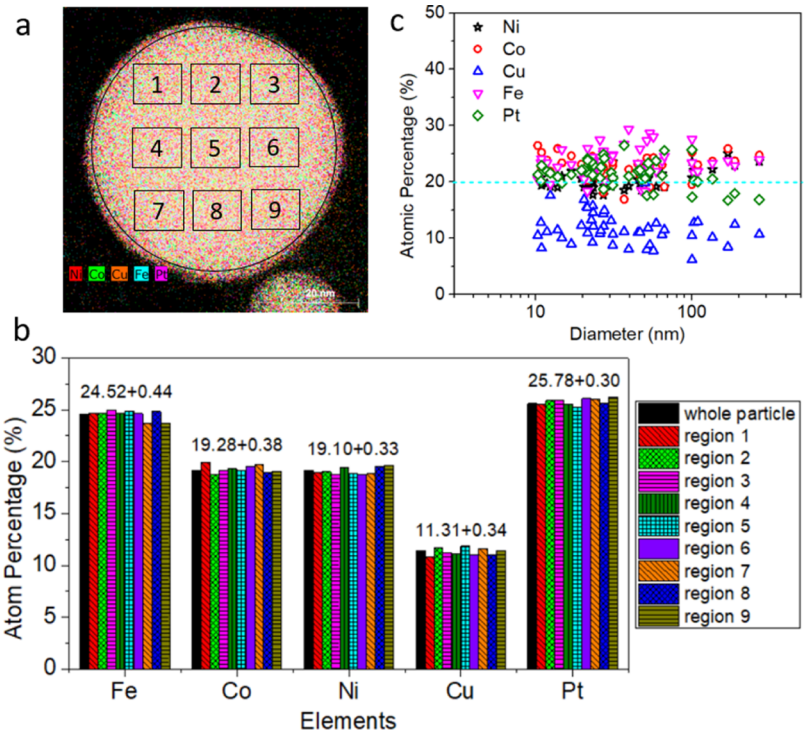

Figure 3. Composition analysis of HEA nanoparticles: (a) HAADF EDS image of the HEA nanoparticle; (b) atomic percentages of five elements in different regions of the HEA nanoparticle in (a); and (c) statistical distributions for atomic percentages of each elements for nanoparticles with different diameters.

to 0.9×10^6 #/cm^3 (Figure 2c), but because we have already eliminated coagulation as too slow, this decrease results from thermophoretic losses from the reactor. These results show that the nanoparticles have a number average diameter of ~59 nm, which is smaller than the average size (92 nm) of aerosol particles before heat treatment. The decrease in particle size is due to shrinking and densification of the aerosol particles caused by thermal decomposition and hydrogen reduction of metal salts to metals. However, the generated HEA nanoparticles have a geometric standard deviation of 1.88, slightly larger than that of the corresponding metal salt aerosol particles without heat treatment. One possible reason is that gas byproducts released from the thermal decomposition and hydrogen reduction of the on-the-fly aerosol particles were temporarily trapped in the aerosol particles, causing the formation of voids in the nanoparticles, widening the size distribution of the final HEA particles. The presence of the void microstructure in the nanoparticles is observed in the collected STEM images, as shown in Figure S12.

The microstructure of HEA nanoparticles was analyzed using atomic-scale STEM. Figure 2d,e displays a HAADF-STEM image and the corresponding annular bright-field STEM (ABF-STEM) image of an HEA nanoparticle to be investigated. In order to examine how all five metal atoms (Ni, Co, Cu, Fe, and Pt) mix with each other in the single HEA nanoparticle, atomic-scale HAADF-STEM was performed on the red square-labeled regions of the corresponding HEA nanoparticle. The results shown in Figure 2f,h indicate that the nanoparticle has a crystalline structure with some atomic plane distortions. The atomic plane distortion might be attributed to differences between radii (ranging from 123 to 138 pm) of the five different metal atoms used (Table S1). The formation of the crystalline structure also indicates that the crystallization process was relatively fast compared to the residence time of the aerosol particles. Moreover, as shown in Figure 2g, the fast Fourier transform (FFT) analysis recorded along the ⟨100⟩ zone axis shows six diffraction spots rendering two *d*-spacings of 1.98 and 1.33 Å, belonging to two lattice planes {200} and {220}, respectively, suggesting that the HEA nanoparticle is compatible with the fcc crystalline structure. This observation is in accordance with the XRD data shown in Figure S2 and is also consistent with the result obtained for the HEA nanoparticles fabricated using the CTS technique reported in our previous study.[2]

Note that the five-element HEA nanoparticles investigated here contains four metal elements with similar atomic masses (Ni, Co, Cu, and Fe) and one element with a relatively large atomic mass (Pt) (Table S2). Typically, atoms having a large atomic mass have a larger interaction cross section and result in higher brightness in the *Z*-contrast STEM image. As shown in Figure 2f,i, there are a lot of bright dots randomly distributed in the matrix. These bright dots could be attributed to Pt atoms in the HEA nanoparticle. The uniform distribution of Pt atoms reflects the atomic-level mixing of the metal elements in the nanoparticle. This result suggests that Pt atoms did not cluster together leading to phase separation but instead, they remain mixed perfectly randomly with four other types of metal atoms in the HEA nanoparticles during the high-temperature treatment.

Because it is difficult to distinguish Ni, Co, Cu, and Fe atoms in the atomic-scale STEM images as shown above, we measured the atomic ratios for the five atoms at various areas (Figure 3a) of the same nanoparticles using the data collected by EDS mapping analysis so as to further investigate how different types of atoms mix in the single nanoparticle. The result shown in Figure 3b indicates that for all the nine

https://dx.doi.org/10.1021/acs.langmuir.9b03392
Langmuir 2020, 36, 1985−1992

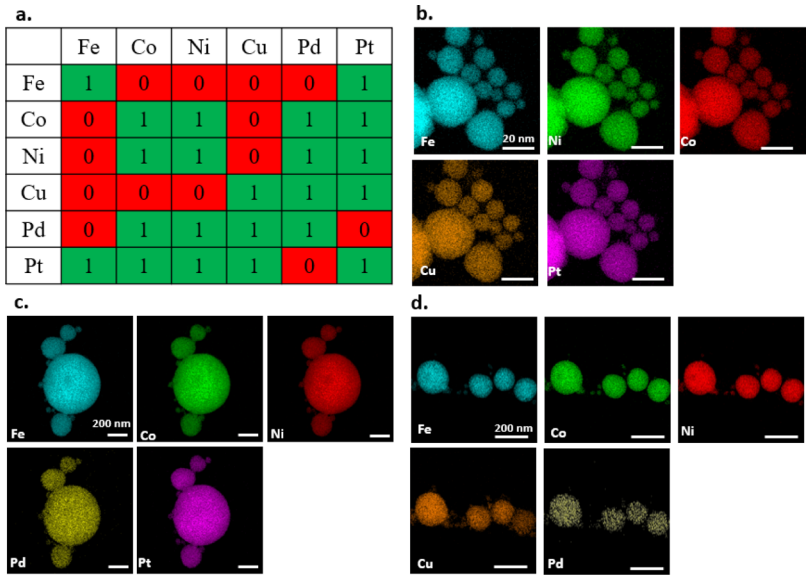

Figure 4. Aerosol processing: a generic approach for HEA nanoparticle synthesis. (a) Miscibility between binary elemental combinations with a 1:1 ratio and data obtained from the ASM Alloy Phase Diagram Database (1 represents the formation of an alloy or intermetallic compound, 0 represents that two metals are immiscible); several types of HEA nanoparticles synthesized: (b) NiCoFeCuPt, (c) NiCoFePdPt, and (d) NiCoCuFePd.

regions examined, the atomic percentage of each element is similar to that of the same element in the whole particle (19.16% for Ni, 19.19% for Co, 11.45% for Cu, 24.59% for Fe, and 25.60% for Pt), confirming the compositional uniformity throughout the whole nanoparticle. Furthermore, we also investigated how the particle size affects the elemental composition in each particle. One example of EDS mapping data containing multiple particles with different sizes is exhibited in Figure S13. We measured the elemental compositions for each particle with the corresponding size, and the results are plotted in Figure 3c. The calculated average elemental composition is listed as follows: Ni: 20.55% + 1.65%; Co: 22.53% + 2.01%; Cu: 11.93% + 3.04%; Fe: 23.54% + 2.63%; and Pt: 21.45% + 2.29%. This result demonstrates that the compositional variation (<~3.00%) of the atomic percentage of each element for different particles is very small, indicating that the particle size does not affect the atomic ratios in different particles. This ~3% compositional variation of the HEA nanoparticles synthesized here is much better than the compositional uniformity of our previously reported CTS technique (10%)[2] and lithography-based technique (50%).[9] The compositional uniformity of HEA nanoparticles generated here might be attributed to the small confinement volume and the homogeneous nature of the thermal field which all particles experience, unlike bulk processing which may have significant thermal gradients. Considering that physical and chemical properties of HEA nanoparticles are greatly affected by their elemental compositions, the HEA nanoparticles with such small variations synthesized by our aerosol technique demonstrate great potential for a broad range of applications.

Generality of the Aerosol Technique. We demonstrate that this aerosol-assisted process offers a generic approach toward synthesis of HEA nanoparticles. Here, we investigate the synthesis of HEA nanoparticles with various combinations of elements including Fe, Co, Ni, Cu, Pd, and Pt. Table S2 shows the standard reduction potentials for all the metal ions used in this study. Because most of the metal elements investigated in this study have relatively low standard potentials, thermal heating is required to reduce the metal salt precursors by hydrogen gas. Hydrogen reduction of metal nitrate precursors in our experiment can be written as

$$M(NO_3)_2 + 2H_2 \rightarrow M + 2NO_2 \uparrow + 2H_2O\uparrow$$

The conversion of metal salt precursor to metallic particles contains two steps: diffusion of hydrogen molecules into the aerosol particles and reduction of metal salt precursors by hydrogen molecules. Because the residence time of the particles in the high-temperature reaction zone is extremely fast (~3 s), we examine if both the diffusion of hydrogen molecules and the hydrogen reactions are kinetically favorable. Previous studies have shown that hydrogen molecules can diffuse through the interstitials in metals. The diffusion coefficient of hydrogen interstitials in the fcc Fe metal is $D \approx 7 \times 10^{-5}$ cm^2/s at room temperature (25 °C),[21] which yields a characteristic diffusion length of ~2×10^5 nm ($d^2 = 6Dt$)[14] within 1 s. Because the diameter of the particles (<10^3 nm) is much smaller than the characteristic diffusion distance and the diffusion process considered at higher temperature (1100 °C), the diffusion of hydrogen should not be rate-limiting. Previous slow heating experiments have reported that most of the metal salt precursors can be reduced to metals at temperatures ranging from 200 to 550 °C.[22] Among all the metal salt precursors investigated in this study, iron is the most reactive metal and has the lowest standard reduction potential. Although we cannot find the kinetic parameters for metal salt reduction, researchers have studied the reduction of iron oxide powers by hydrogen at elevated temperatures.[23] The reduction of the metal salt precursor was estimated based on this study. Assuming the reduction of metal salt precursor particles following a shrink core model with a reaction kinetics described by the equation $(1 - (1 - \alpha)^{1/3})^2 = k(T)t$, where α is the conversion and $k(T)$ is the reaction rate at a reaction temperature T.[23] The complete conversion time for iron nitrate is less than 0.04 s at a reaction temperature of 1100 °C, which is much shorter than our residence time. Hence, elevated temperature fastens the kinetics of the hydrogen

https://dx.doi.org/10.1021/acs.langmuir.9b03392
Langmuir 2020, 36, 1985−1992

reduction of metal salt precursors and enables the completion of the conversion of the metal salt to metallic phase in less than 3 s.

Figure 4a shows the miscibility between binary elemental combinations and the data obtained from the ASM alloy phase diagram database. The result suggests, for example, that Cu prefers to separate with Fe, Co, or Ni thermodynamically. We show that the aerosol-assisted processing technique enables the uniform mixing of different elements via kinetically controlled synthesis, even though these elements are not mixable thermodynamically. In this study, we have successfully synthesized FeCoNiCuPt, FeCoNiPdPt, and FeCoNiCuPd HEA nanoparticles. The elemental distributions for each type of HEA nanoparticles are investigated using EDS analysis, as shown in Figure 4b–d, confirming the uniform mixing for all elements for each type of HEA nanoparticle.

CONCLUSIONS

We have demonstrated an aerosol droplet-mediated technique toward scalable synthesis of HEA nanoparticles with atomic-level mixing of immiscible metal elements. The aqueous solution containing desired different metal salts was nebulized into millions of aerosol droplets with a diameter of less than 1 μm, and fast heating and fast quenching treatment was exerted on these on-the-fly droplets with each droplet acting as a nanoreactor to produce a single HEA nanoparticle. An atomic-level STEM study coupled with EDS analysis reveals that all metal elements in the nanoparticles are mixed together at an atomic level. We believe that this facile and flexible aerosol droplet-mediated synthesis technique advances the field of HEA nanoparticles and also demonstrates the potential to transcend fundamental research to industrial application.

EXPERIMENTAL SECTION

Materials. Nickel nitrate hexahydrate [$Ni(NO_3)_2{\cdot}6H_2O$, ≥99% pure], cobalt nitrate hexahydrate [$Co(NO_3)_2{\cdot}6H_2O$, ≥99% pure], iron nitrate nonahydrate [$Fe(NO_3)_3{\cdot}9H_2O$, ≥99% pure], copper nitrate trihydrate [$Cu(NO_3)_2{\cdot}3H_2O$, ≥99% pure], palladium chloride ($PdCl_2$, ≥99% pure), and chloroplatinic acid (H_2PtCl_6, 99%) were all purchased from Sigma-Aldrich. All the chemicals were used as received.

Precursor Preparation. The precursor solution was prepared by dissolving an equimolar amount of metal salts in de-ionized water. The total concentration of the metal salts in the solutions was 0.02 M.

Aerosol Droplet-Mediated Synthesis Technique. HEAs were synthesized using a one-step aerosol spray pyrolysis technique. A schematic of the aerosol reactor including details of the geometry, flow rates, operation pressure, and temperature profiles can be found in Figure S1. The experiment consists of a Collison nebulizer (BGI Inc.), a silica dryer, a silica tubular reactor heated by two combined tube furnace, and a membrane filter (Millipore, material: polycarbonate, pore size: 0.4 μm). In a typical experiment, the prepared precursor solution was loaded into the atomizer and was nebulized into small aerosol droplets using a 10% H_2/90% Ar mixture gas with a pressure of 30 psi. These droplets carried by the mixture gas were first passed through the silica dryer, where the water solvent evaporated from the droplets. Following the water solvent removal, the resulting dry aerosol particles moved into the high-temperature tubular furnace reactor (diameter: 2 cm; heating length: 60 cm, set temperature: 1100 °C), where fast heating led to the rapid decomposition and reduction of the metal salts to metals, and the subsequent fast cooling resulted in the HEA formation. The products were collected with a membrane filter collector, which blew cooling air to achieve fast quenching of the product. Under scale-up conditions, the membrane filters would be replaced by bag filters or electrostatic precipitators. The aerosol flow rate was ∼3 L/min, which was measured at the end of the sample collector. Thus, based on the geometry of the aerosol reactor and the gas flow rate, the calculated residence time of the droplets in the high-temperature reactor was about 3 s.

Finite Element Simulation of Temperature Profile of the Gas Flow in the Tubular Reactor. In order to estimate the temperature profiles of the aerosol gas flow in the tubular reactor, a finite-element simulation of the aerosol synthesis process was implemented using COMSOL Multiphysics software. The model including the tubular reactor and sample collector with the aerosol flow was constructed. We assumed that the temperature on the surface of the tubular reactor in the heating zone (length: 60 cm) was 1100 °C, and the sample collector cooled with the cold air retained a temperature of 25 °C on its surface, with a gas flow rate of 3 lpm. The calculated Reynold number was ∼30. We expect the flow to be laminar; thus, the non-isothermal laminar flow module in the software was used for the model.

Characterization. The morphology, microstructure, and composition of the HEA nanoparticles were examined by SEM, TEM, STEM, EDS, and XRD. SEM samples were prepared by directly casting the powder sample onto the conductive carbon tape attached to the SEM sample holder. TEM samples were prepared by redispersing and sonicating the powder samples in ethanol and depositing the suspension onto the TEM grids. SEM images were taken with an NS450 scanning electron microscope at an acceleration voltage of 18 kV. A JEOL ARM-200CF was used to image HEA nanoparticles deposited on a lacey carbon Mo grid. HAADF and ABF images were acquired using a spherical aberration-corrected JEOL JEM-ARM 200CF scanning transmission electron microscope with a cold field emission gun operating at 200 kV, with a 22 mrad convergence angle. Images were taken using an Orius CCD camera with 512 × 512 scanning resolution. EDS analyzes and elemental mapping were performed in the STEM mode (Thermo Fisher Scientific Titan Themis 300 Instrument, fitted with an X-FEG electron source, 3 lens condenser systems, and S-Twin objective lens) at 300 kV, utilizing a Thermo Fisher Scientific SuperX system equipped with 4 × 30 mm^2 window-less silicon drift detectors symmetrically surrounding the specimen with a total collection angle of 0.7 srad, by scanning the selected area from the specimens. Elemental mapping by plotting the net X-ray counts was performed with an electron beam probe current of 550 pA at 1024 × 1024 frame resolution, a dwell time of 30 μs/pixel, and scanning multiple frames resulting in effective total acquisition time between 3 and 10 min. EDS spectra were extracted from the elemental maps and by direct spectra acquisition from selected areas. Elemental concentrations were calculated using the Cliff–Lorimer ratio technique[24] using calculated k-factors, which have been verified experimentally to incorporate an error of less than ±3% by analyzing standard specimens with known composition of SiO_2, SiC, TiO_2, and NiO and correcting for absorption. The minimum error in determining the elemental concentrations in the studied specimens is estimated from the statistical uncertainty in measuring the X-ray peak intensities which was less than 5% relative. The EDS spectra were used to quantify the composition of the HEA particles deposited on a lacey carbon Au grid. The XRD analysis was performed on the nanoparticles collected on the membrane filter.

On-Line Particle Size and Concentration Analysis. The size distributions and total concentration of metal precursor aerosol particles and HEA aerosol particles were analyzed using a DMA (TSI, model 3081) coupled with a CPC (TSI, model 3776) on-line size analysis system (DMA–CPC). The operation principles can be found in our previous publication.[19] The size distribution of the dried aerosol particles containing multiple metal salts was directly measured after the silica drying and before heating the tube. The size distribution of HEA nanoparticles was measured with the DMA–CPC at the exit of the heated reactor tube.

https://dx.doi.org/10.1021/acs.langmuir.9b03392
Langmuir 2020, 36, 1985–1992

■ ASSOCIATED CONTENT

Supporting Information

The Supporting Information is available free of charge at https://pubs.acs.org/doi/10.1021/acs.langmuir.9b03392.

Aerosol reactor design and flow dynamics analysis; XRD pattern of HEA nanoparticles; EDS spectrum for HEA nanoparticles; vapor pressures for different metals; size distribution of dried aerosol particles containing metal salt mixtures measured using a DMA−CPC system; temperature profile of the aerosol gas flow simulated by COMSOL; effect of the cooling rate on the microstructure of multicomponent metal nanoparticles; characteristic coagulation time and sintering time calculation; HAADF and BF images of NiCoFeCuPt HEA nanoparticles showing the hollow sphere shape; physical properties of different metals investigated in this study; standard reduction potentials for different metals; and estimation on the yield of the aerosol process (PDF)

■ AUTHOR INFORMATION

Corresponding Authors

Reza Shahbazian-Yassar − *University of Illinois at Chicago, Chicago, Illinois 60607, United States;* orcid.org/0000-0002-7744-4780; Email: rsyassar@uic.edu

Michael R. Zachariah − *University of California Riverside, Riverside, California 92521, United States;* orcid.org/0000-0002-4115-3324; Email: mrz@engr.ucr.edu

Authors

Yong Yang − *University of California Riverside, Riverside, California 92521, United States; University of Maryland, College Park, Maryland 20742, United States;* orcid.org/0000-0001-5169-1479

Boao Song − *University of Illinois at Chicago, Chicago, Illinois 60607, United States;* orcid.org/0000-0003-3124-3235

Xiang Ke − *University of California Riverside, Riverside, California 92521, United States*

Feiyu Xu − *University of California Riverside, Riverside, California 92521, United States; University of Maryland, College Park, Maryland 20742, United States*

Krassimir N. Bozhilov − *University of California Riverside, Riverside, California 92521, United States*

Liangbing Hu − *University of Maryland, College Park, Maryland 20742, United States;* orcid.org/0000-0002-9456-9315

Complete contact information is available at: https://pubs.acs.org/10.1021/acs.langmuir.9b03392

Notes

The authors declare no competing financial interest.

■ ACKNOWLEDGMENTS

The financial support for this research comes from an ONR MURI grant and the NSF Scalable Nanomanufacturing project no. 1635221. R.S.-Y. and B.S. acknowledge the funding from NSF-DMR-1809439. This work made use of instruments in the Electron Microscopy Service (Research Resources Center, UIC) and the Central Facility for Advanced Microscopy and Microanalysis at UC, Riverside. The acquisition of the UIC JEOL JEM-ARM200CF was supported by an MRI-R2 grant from the National Science Foundation (award no. DMR-0959470).

■ REFERENCES

(1) Chen, P.-C.; Liu, M.; Du, J. S.; Meckes, B.; Wang, S.; Lin, H.; Dravid, V. P.; Wolverton, C.; Mirkin, C. A. Interface and heterostructure design in polyelemental nanoparticles. *Science* **2019**, *363*, 959−964.

(2) Yao, Y.; Huang, Z.; Xie, P.; Lacey, S. D.; Jacob, R. J.; Xie, H.; Chen, F.; Nie, A.; Pu, T.; Rehwoldt, M.; Yu, D.; Zachariah, M. R.; Wang, C.; Shahbazian-Yassar, R.; Li, J.; Hu, L. Carbothermal shock synthesis of high-entropy-alloy nanoparticles. *Science* **2018**, *359*, 1489−1494.

(3) Takahashi, M.; Koizumi, H.; Chun, W.-J.; Kori, M.; Imaoka, T.; Yamamoto, K. Finely controlled multimetallic nanocluster catalysts for solvent-free aerobic oxidation of hydrocarbons. *Sci. Adv.* **2017**, *3*, No. e1700101.

(4) Yeh, J.-W.; Chen, S.-K.; Lin, S.-J.; Gan, J.-Y.; Chin, T.-S.; Shun, T.-T.; Tsau, C.-H.; Chang, S.-Y. Nanostructured high-entropy alloys with multiple principal elements: novel alloy design concepts and outcomes. *Adv. Eng. Mater.* **2004**, *6*, 299−303.

(5) Ye, Y. F.; Wang, Q.; Lu, J.; Liu, C. T.; Yang, Y. High-entropy alloy: challenges and prospects. *Mater. Today* **2016**, *19*, 349−362.

(6) Buck, M. R.; Bondi, J. F.; Schaak, R. E. A total-synthesis framework for the construction of high-order colloidal hybrid nanoparticles. *Nat. Chem.* **2012**, *4*, 37.

(7) Nie, Z.; Li, W.; Seo, M.; Xu, S.; Kumacheva, E. Janus and ternary particles generated by microfluidic synthesis: design, synthesis, and self-assembly. *J. Am. Chem. Soc.* **2006**, *128*, 9408−9412.

(8) Ganguli, A. K.; Ganguly, A.; Vaidya, S. Microemulsion-based synthesis of nanocrystalline materials. *Chem. Soc. Rev.* **2010**, *39*, 474−485.

(9) Chen, P.-C.; Liu, X.; Hedrick, J. L.; Xie, Z.; Wang, S.; Lin, Q.-Y.; Hersam, M. C.; Dravid, V. P.; Mirkin, C. A. Polyelemental nanoparticle libraries. *Science* **2016**, *352*, 1565−1569.

(10) Li, Z.; Pradeep, K. G.; Deng, Y.; Raabe, D.; Tasan, C. C. Metastable high-entropy dual-phase alloys overcome the strength−ductility trade-off. *Nature* **2016**, *534*, 227.

(11) Santodonato, L. J.; Zhang, Y.; Feygenson, M.; Parish, C. M.; Gao, M. C.; Weber, R. J.; Neuefeind, J. C.; Tang, Z.; Liaw, P. K. Deviation from high-entropy configurations in the atomic distributions of a multi-principal-element alloy. *Nat. Commun.* **2015**, *6*, 5964.

(12) Shatrova, N.; Yudin, A.; Levina, V.; Dzidziguri, E.; Kuznetsov, D.; Perov, N.; Issi, J.-P. Elaboration, characterization and magnetic properties of cobalt nanoparticles synthesized by ultrasonic spray pyrolysis followed by hydrogen reduction. *Mater. Res. Bull.* **2017**, *86*, 80−87.

(13) Liang, Y.; Hou, H.; Yang, Y.; Glicksman, H.; Ehrman, S. Conductive One-and Two-Dimensional Structures Fabricated Using Oxidation-Resistant Cu−Sn Particles. *ACS Appl. Mater. Interfaces* **2017**, *9*, 34587−34591.

(14) Wu, C.; Lee, D.; Zachariah, M. R. Aerosol-based self-assembly of nanoparticles into solid or hollow mesospheres. *Langmuir* **2010**, *26*, 4327−4330.

(15) Atkinson, J. D.; Fortunato, M. E.; Dastgheib, S. A.; Rostam-Abadi, M.; Rood, M. J.; Suslick, K. S. Synthesis and characterization of iron-impregnated porous carbon spheres prepared by ultrasonic spray pyrolysis. *Carbon* **2011**, *49*, 587−598.

(16) Chen, Y.; Guo, F.; Jachak, A.; Kim, S.-P.; Datta, D.; Liu, J.; Kulaots, I.; Vaslet, C.; Jang, H. D.; Huang, J.; Kane, A.; Shenoy, V. B.; Hurt, R. H. Aerosol synthesis of cargo-filled graphene nanosacks. *Nano Lett.* **2012**, *12*, 1996−2002.

(17) Yang, Y.; Romano, M.; Feng, G.; Wang, X.; Wu, T.; Holdren, S.; Zachariah, M. R. Growth of Sub-5 nm Metal Nanoclusters in Polymer Melt Aerosol Droplets. *Langmuir* **2018**, *34*, 585−594.

(18) Yang, Y.; Ghildiyal, P.; Zachariah, M. Rapid and Scalable Synthesis of Sub-10 nm Metal Nanoparticles in On-the-Fly Aerosols. *256th ACS National Meeting*; American Chemical Society: Boston, MA, 2018.

(19) Zong, Y.; Jacob, R. J.; Li, S.; Zachariah, M. R. Size Resolved High Temperature Oxidation Kinetics of Nano-Sized Titanium and Zirconium Particles. *J. Phys. Chem. A* **2015**, *119*, 6171−6178.

(20) Zhao, J.; Baibuz, E.; Vernieres, J.; Grammatikopoulos, P.; Jansson, V.; Nagel, M.; Steinhauer, S.; Sowwan, M.; Kuronen, A.; Nordlund, K.; Djurabekova, F. Formation mechanism of Fe nanocubes by magnetron sputtering inert gas condensation. *ACS Nano* **2016**, *10*, 4684−4694.
(21) Wipf, H. Solubility and diffusion of hydrogen in pure metals and alloys. *Phys. Scr.* **2001**, *2001*, 43.
(22) Luidold, S.; Antrekowitsch, H. Hydrogen as a reducing agent: State-of-the-art science and technology. *Jom* **2007**, *59*, 20−26.
(23) Lin, H.-Y.; Chen, Y.-W.; Li, C. The mechanism of reduction of iron oxide by hydrogen. *Thermochim. Acta* **2003**, *400*, 61−67.
(24) Cliff, G.; Lorimer, G. W. The quantitative analysis of thin specimens. *J. Microsc.* **1975**, *103*, 203−207.

https://dx.doi.org/10.1021/acs.langmuir.9b03392
Langmuir 2020, 36, 1985−1992